Optimization and Structural Characterization of W/Al $_2$ O $_3$ Nanolaminates Grown Using Atomic Layer Deposition Techniques

6 AUTHORS, INCLUDING:

David C. Johnson
University of Oregon
273 PUBLICATIONS **2,592** CITATIONS

S.M. George
University of Colorado at Boulder
183 PUBLICATIONS **8,164** CITATIONS

Optimization and Structural Characterization of W/Al$_2$O$_3$ Nanolaminates Grown Using Atomic Layer Deposition Techniques

Z. A. Sechrist,[†] F. H. Fabreguette,[†] O. Heintz,[‡] T. M. Phung,[§] D. C. Johnson,[§] and
S. M. George*,[†,||]

Department of Chemistry and Biochemistry and Department of Chemical and Biological Engineering, University of Colorado, Boulder, Colorado 80309; Laboratoire de Recherches sur la Réactivité des Solides, UMR 5613, Université de Bourgogne, 9 Avenue A. Savary BP 47870, 21078 Dijon Cedex, France; and Department of Chemistry and Materials Science Institute, University of Oregon, Eugene, Oregon 97403

W/Al$_2$O$_3$ nanolaminates were fabricated using atomic layer deposition (ALD) techniques. ALD of tungsten was performed using alternating exposures of WF$_6$ and Si$_2$H$_6$. ALD of Al$_2$O$_3$ was performed using alternating exposures of Al(CH$_3$)$_3$ and H$_2$O. The fabrication of optimum nanolaminates was very dependent on nucleation during the ALD of each layer. The nucleation of Al$_2$O$_3$ ALD on W surfaces and W ALD on Al$_2$O$_3$ surfaces was examined using quartz crystal microbalance investigations. Al$_2$O$_3$ ALD on W nucleated easily during the first Al(CH$_3$)$_3$/H$_2$O reaction cycle. In contrast, W ALD nucleation on Al$_2$O$_3$ required multiple WF$_6$/Si$_2$H$_6$ reaction cycles and was very sensitive to the Si$_2$H$_6$ exposure. The W ALD nucleation required at least six or seven WF$_6$/Si$_2$H$_6$ reaction cycles. The optimum reaction parameters for nucleation were utilized to fabricate W/Al$_2$O$_3$ nanolaminates with a total targeted thickness of ∼1000 Å that were composed of various numbers of bilayers. Transmission electron microscopy (TEM) images revealed very well defined two-bilayer and four-bilayer W/Al$_2$O$_3$ nanolaminates grown at 177 °C. Depth-profile secondary ion mass spectrometry (SIMS) measurements confirmed the composition of the W/Al$_2$O$_3$ nanolaminates. Both the TEM and SIMS results showed that sharper interfaces were observed when W ALD nucleates on Al$_2$O$_3$, and rougher interfaces were observed when Al$_2$O$_3$ ALD nucleates on W. X-ray reflectivity (XRR) investigations indicated that the W/Al$_2$O$_3$ nanolaminates were much thicker than the ∼1000 Å target for the total thickness when the W/Al$_2$O$_3$ nanolaminates were composed of a larger number of bilayers. These results were consistent with much lower than expected film densities for the thin Al$_2$O$_3$ ALD nanolayers. Atomic force microscope studies revealed that the surface roughness of W/Al$_2$O$_3$ nanolaminates was lower at lower growth temperatures and lower at higher interfacial densities. XRR investigations also revealed a pronounced Bragg peak with a high X-ray reflectivity from 64-bilayer W/Al$_2$O$_3$ nanolaminates grown at 177 °C. The X-ray reflectivity of the 64-bilayer W/Al$_2$O$_3$ nanolaminates grown at 177 °C was constant versus annealing up to 500 °C. The reflectivity then dropped rapidly for annealing at ≥600 °C. This thermal instability will place some limits on the application of W/Al$_2$O$_3$ nanolaminates as thermal barrier coatings and X-ray mirrors.

I. Introduction

Nanolaminates are multilayer films made from alternating layers of different materials with nanometer thicknesses. Nanolaminates may display physical properties that are not simply determined by a "rule of mixtures". These novel mechanical, thermal, electrical, and optical properties typically result when the nanolayer thicknesses are less than the length scale that defines the physical property. For example, high hardness nanolaminate films may result when the nanolayer thickness is less than the slip plane dislocation length.[1,2] Low thermal conductivity nanolaminate films may result when the nanolayer thickness is less than the phonon mean free path.[3,4]

Atomic layer deposition (ALD) has emerged as an excellent technique to fabricate conformal, continuous, and ultrathin films. ALD is based on sequential, self-limiting surface reactions.[5,6] These sequential surface reactions allow the film thickness to be controlled at the atomic scale. ALD growth rates are typically 1−2 Å per surface reaction cycle. Nanolaminates can be fabricated by employing ALD surface reactions for the first material and then switching to ALD surface reactions for the second material.[7] By alternating between these two ALD surface chemistries, nanolaminates can be fabricated with atomic level precision. Many nanolaminates have been fabricated by ALD, including W/Al$_2$O$_3$,[8]

---

* Corresponding author. Phone: 303-492-3398. Fax: 303-492-5894. E-mail: Steven.George@colorado.edu
† Department of Chemistry and Biochemistry, University of Colorado.
‡ Université de Bourgogne.
§ University of Oregon.
|| Department of Chemical and Biological Engineering, University of Colorado.

(1) Veprek, S. *J. Vac. Sci. Technol. A* **1999,** *17,* 2401.
(2) Yashar, P. C.; Sproul, W. D. *Vacuum* **1999,** *55,* 179.
(3) Chen, G.; Neagu, M. *Appl. Phys. Lett.* **1997,** *71,* 2761.
(4) Chen, G. *Phys. Rev. B* **1998,** *57,* 14958.
(5) George, S. M.; Ott, A. W.; Klaus, J. W. *J. Phys. Chem.* **1996,** *100,* 13121.
(6) Suntola, T. *Thin Solid Films* **1992,** *216,* 84.
(7) Kukli, K.; Ihanus, J.; Ritala, M.; Leskela, M. *Appl. Phys. Lett.* **1996,** *68,* 3737.
(8) Costescu, R. M.; Cahill, D. G.; Fabreguette, F. H.; Sechrist, Z. A.; George, S. M. *Science* **2004,** *303,* 989.

ZnO/Al_2O_3,[9,10] HfO_2/ZrO_2,[11] ZrO_2/Al_2O_3,[12] Ta_2O_5/Al_2O_3,[13] GaP/AlP,[14] $ZnSe/CdSe$,[15] HfO_2/Ta_2O_5,[7,16] SiO_2/Al_2O_3,[17] and SiO_2/ZrO_2.[18]

W/Al_2O_3 nanolaminates can be fabricated using W ALD and Al_2O_3 ALD. Al_2O_3 ALD is based on alternating exposures of $Al(CH_3)_3$ [trimethylaluminum (TMA)] and H_2O.[19-21] Al_2O_3 ALD is one of the best studied ALD systems. W ALD is based on alternating exposures of WF_6 and Si_2H_6.[22,23] W ALD utilizes two sequential reactions that produce a single-element W film. The Si_2H_6 plays a sacrificial role to strip fluorine from W. The silicon surface species deposited during the Si_2H_6 exposure are removed from the surface by the subsequent WF_6 exposure.

Many studies have investigated various details of W ALD. Fourier transform infrared (FTIR) studies have monitored the surface species versus the WF_6 and Si_2H_6 exposures.[22] Spectroscopic ellipsometry investigations have measured the W ALD growth rates.[22] Auger electron spectroscopy (AES) studies have examined the kinetics of the WF_6 and Si_2H_6 surface reactions and characterized the W ALD growth rates.[24] AES studies have also examined the details of W ALD nucleation and growth on SiO_2 and Al_2O_3 substrates.[25,26] Mass spectrometer studies have examined the gas-phase reaction products and correlated the evolution of these reaction products with changes in the AES spectrum.[27] Electrical studies have monitored the W ALD film growth using in situ resistivity measurements.[28] Quartz crystal microbalance (QCM) investigations have also measured the mass changes during the WF_6 and Si_2H_6 exposures.[29]

This paper extends beyond the previous studies and examines the growth of W/Al_2O_3 nanolaminates using quartz crystal microbalance (QCM) techniques. W ALD on Al_2O_3 and Al_2O_3 ALD on W were both examined and optimized in a viscous flow reactor to obtain nucleation with a minimum number of reaction cycles. These optimum reaction parameters were then utilized to grow different W/Al_2O_3 nanolaminates. The structure of these W/Al_2O_3 nanolaminates was then thoroughly investigated for the first time by transmission electron microscopy (TEM), secondary ion mass spectrometry (SIMS), atomic force microscopy (AFM), and X-ray reflectivity (XRR) studies. The results of these structural studies reveal interesting interfacial roughnesses and density features that will affect the growth of well-defined W/Al_2O_3 nanolaminates with precise thicknesses. XRR annealing investigations also indicate that the W/Al_2O_3 nanolaminates may have application at high temperatures for thermal barrier coatings and X-ray mirrors.

II. Experimental Section

A. Viscous Flow Reactor. The nanolaminates were grown in a hot wall viscous flow reactor at the University of Colorado. The basic design of this reactor has been described in detail previously.[30] This reactor has two heating zones. These heating zones are defined by 6 and 12 in. long cylindrical heaters from Watlow that were placed around the flow tube. These two heaters were placed in series with one another. The ceramic Watlow heaters were controlled by a Eurotherm 905D PID controller. The cylindrical controlled growth region was 1.5 in. in diameter and 21 in. long.

Pure nitrogen from Air Gas Inc. [99.999%, ultrahigh purity (UHP)] was used as the viscous flow carrier gas. This nitrogen was sent through a Gate Keeper oxygen filter from Aeronex Inc. to limit the oxygen content to <1ppb. Three mass flow controllers from MKS Inc. introduced nitrogen into the reactor. The total N_2 flow was ~200 sccm. The ALD reactor was pumped by an Alcatel 2010 SD dual-stage rotary vane mechanical pump. The total pressure in the growth region was ~1 Torr and the N_2 gas flow rate was ~1m/s.

The reactant gases were pulsed into the nitrogen flow with computer-controlled pneumatic valves from Swagelok. The reactant gases were entrained in the nitrogen flow and transported through the ALD reactor. The reactants were all maintained at room temperature. Each reactant had a higher vapor pressure than the ~1 Torr pressure in the gas lines and the reactor. The reactants could easily be added to the nitrogen carrier gas using this pressure gradient. The stainless steel tubing carrying the reactants to the growth area was heated to ~60 °C to avoid any possible condensation.

After the reactant gases reacted to completion with the available surface sites, the nitrogen entrained the excess reactant and products. A purge time after each reactant exposure allowed for the nitrogen to sweep the reactor clean of reactive gases and avoid chemical vapor deposition. The reactant lines were pumped separately by Alcatel 2005 dual-stage rotary vane mechanical pumps.

B. Surface Chemistry and Precursors. Al_2O_3 ALD is a model ALD system and has been explored by numerous investigations.[19-21,30-33] Surface exposures of $Al(CH_3)_3$ [trimethylaluminum (TMA)] and H_2O lead to Al_2O_3 ALD growth at ~1.2 Å/cycle.[20,30]

(9) Elam, J. W.; Sechrist, Z. A.; George, S. M. *Thin Solid Films* **2002**, *414*, 43.

(10) Jensen, J. M.; Oelkers, A. B.; Toivola, R.; Johnson, D. C.; Elam, J. W.; George, S. M. *Chem. Mater.* **2002**, *14*, 2276.

(11) Kim, H. S.; McIntyre, P. C.; Saraswat, K. C. *J. Mater. Res.* **2004**, *19*, 643.

(12) Besling, W. F. A.; Young, E.; Conard, T.; Zhao, C.; Carter, R.; Vandervorst, W.; Caymax, M.; De Gendt, S.; Heyns, M.; Maes, J.; Tuominen, M.; Haukka, S. *J. Non-Cryst. Solids* **2002**, *303*, 123.

(13) Kukli, K.; Ihanus, J.; Ritala, M.; Leskela, M. *J. Electrochem. Soc.* **1997**, *144*, 300.

(14) Ishii, M.; Iwai, S.; Kawata, H.; Ueki, T.; Aoyagi, Y. *J. Cryst. Growth* **1997**, *180*, 15.

(15) Solanki, R.; Huo, J.; Freeouf, J. L.; Miner, B. *Appl. Phys. Lett.* **2002**, *81*, 3864.

(16) Zhang, H.; Solanki, R. *J. Electrochem. Soc.* **2001**, *148*, F63.

(17) Hausmann, D.; Becker, J.; Wang, S. L.; Gordon, R. G. *Science* **2002**, *298*, 402.

(18) Zhong, L. J.; Chen, F.; Campbell, S. A.; Gladfelter, W. L. *Chem. Mater.* **2004**, *16*, 1098.

(19) Ott, A. W.; Klaus, J. W.; Johnson, J. M.; George, S. M. *Thin Solid Films* **1997**, *292*, 135.

(20) Ott, A. W.; McCarley, K. C.; Klaus, J. W.; Way, J. D.; George, S. M. *Appl. Surf. Sci.* **1996**, *107*, 128.

(21) Dillon, A. C.; Ott, A. W.; Way, J. D.; George, S. M. *Surf. Sci.* **1995**, *322*, 230.

(22) Klaus, J. W.; Ferro, S. J.; George, S. M. *Thin Solid Films* **2000**, *360*, 145.

(23) Klaus, J. W.; Ferro, S. J.; George, S. M. *Appl. Surf. Sci.* **2000**, *162*, 479.

(24) Elam, J. W.; Nelson, C. E.; Grubbs, R. K.; George, S. M. *Surf. Sci.* **2001**, *479*, 121.

(25) Elam, J. W.; Nelson, C. E.; Grubbs, R. K.; George, S. M. *Thin Solid Films* **2001**, *386*, 41.

(26) Grubbs, R. K.; Nelson, C. E.; Steinmetz, N. J.; George, S. M. *Thin Solid Films* **2004**, *467*, 16.

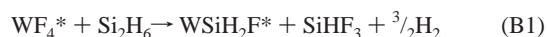(27) Grubbs, R. K.; Steinmetz, N. J.; George, S. M. *J. Vac. Sci. Technol. B* **2004**, *22*, 1811.

(28) Schuisky, M.; Elam, J. W.; George, S. M. *Appl. Phys. Lett.* **2002**, *81*, 180.

(29) Fabreguette, F. H.; Sechrist, Z. A.; Elam, J. W.; George, S. M. *Thin Solid Films*, in press.

(30) Elam, J. W.; Groner, M. D.; George, S. M. *Rev. Sci. Instrum.* **2002**, *73*, 2981.

The mechanism of Al_2O_3 ALD consists of two self-limiting, gas−surface reactions. The two surface reactions are[19−21]

$$AlOH* + Al(CH_3)_3 \rightarrow AlOAl(CH_3)_2* + CH_4 \qquad (A)$$

$$Al(CH_3)* + H_2O \rightarrow AlOH* + CH_4 \qquad (B)$$

where the asterisks indicate the surface species. The trimethylaluminum (Akzo Nobel) was semiconductor grade and had a vapor pressure of ∼10 Torr at room temperature. The oxidant was HPLC grade Optima H_2O (Fisher Inc.). Water has a vapor pressure ∼20 Torr at room temperature.

Tungsten ALD was accomplished using alternating exposures of tungsten hexafluoride (WF_6) and disilane (Si_2H_6). W ALD has been examined by numerous investigations.[22−28] The surface chemistry for W ALD is expressed most accurately by[27]

$$WSiHSiH_3* + 2WF_6 \rightarrow WWWF_4* + 2SiF_4 + {}^3/_2H_2 + HF \quad (A)$$

$$WF_4* + Si_2H_6 \rightarrow WSiH_2F* + SiHF_3 + {}^3/_2H_2 \qquad (B1)$$

$$WSiH_2F* + {}^1/_2Si_2H_6 \rightarrow WSiHFSiH_3* + {}^1/_2H_2 \qquad (B2)$$

W ALD yields growth rates of 4.5−6.0 Å/cycle at growth temperatures from 177 to 325 °C.[29] The 99.9% tungsten hexafluoride gas (Aldrich Chemical Co. Inc.) had a vapor pressure ∼850 Torr at room temperature. The 99.99% disilane (Scott Specialty Gas) had a vapor pressure of ∼2500 Torr at room temperature.

The nanolaminate films were all grown on hydrogen fluoride (HF)−last Si(100) substrates. The silicon samples were first cleaned in a heated piranha solution (70% sulfuric acid and 30% hydrogen peroxide). The Si(100) wafers were then placed in 5% HF solution for 1 min prior to the final rinse in Optima H_2O.

C. Quartz Crystal Microbalance and Atomic Force Microscope. The quartz crystal microbalance (QCM) can measure mass deposition with a sensitivity as low as ∼0.6 ng/cm². The QCM oscillator was a polished gold-coated quartz crystal from Maxtek Inc. The quartz crystal oscillates in a shear mode at ∼6 MHz. The Maxtek TM 400 thickness monitor measured small changes in the oscillatory period. These changes can be converted into mass per area using the Sauerbrey equation.[34]

To avoid deposition on the backside of the QCM sensor, the water cooling lines on the QCM housing were converted into nitrogen carriers.[30] UHP nitrogen was flowed into the crystal housing to prevent backside deposition. The temperature of the QCM housing was monitored with a thermocouple mounted on the QCM housing. Excellent temperature control of ±0.02 °C was achieved using the Eurotherm 905D PID controller.

Atomic force microscope (AFM) measurements were performed using a Park Autoprobe CP instrument from Thermomicroscopes. This AFM was positioned on an air table from Integrated Dynamics Engineering. All roughness measurements were performed in noncontact mode. The same noncontact tip was used for an entire experiment. Data were only compared with other data obtained with the same AFM tip.

The tips utilized were the B tips on the noncontact ultralevers from Thermomicroscopes. All scans were performed over an area of 1 μm × 1 μm at a scan rate of 1 Hz. Flattening was used to compensate for piezoelectric distortion of the sample image.

Second-order fitting for the fast scan direction and first-order fitting for the slow scan direction were used for all samples. The roughness of various samples was compared using the root-mean-squared (rms) roughness.

D. X-ray Diffraction and X-ray Reflectivity. X-ray diffraction (XRD) and X-ray reflectivity (XRR) to obtain X-ray reflectivity intensities and study annealing behavior were performed at the University of Colorado. These X-ray measurements were performed on a Bede Scientific Inc. D1 instrument. The Bede D1 used a Max Flux graded mirror from Osmic Inc. to monochromate and focus X-rays from the Cu-tube point source. The XRD scans were all collected in glancing incidence mode to minimize underlying substrate effects. The incident angle was set at 1.5° and the detection angle was scanned throughout the desired range. The X-ray tube filament current was 40 mA and the accelerating voltage was 40 kV.

For the XRR data, the X-ray tube filament current was 30 mA and the accelerating voltage was 35 kV. The XRR measurements characterized the superlattice structure of the nanolaminate. The Kiessig oscillations and Bragg peaks of various orders were fit using the REFS genetic algorithm program from Bede Scientific Inc. These fits yielded the film thicknesses, film densities, and interfacial roughness.

XRR measurements were also performed at the University of Oregon to measure the layer thicknesses and total film thickness for a variety of W/Al₂O₃ nanolaminates grown to obtain a target thickness of ∼1000 Å. The XRR experiments were performed using a Philips X′Pert five-circle diffractometer. The incident beam of Cu Kα radiation was conditioned by a Soller slit assembly. Measurements were taken in a $\theta−2\theta$ geometry from $\theta = 0.1$ to $\theta = 5°$ with an X-ray tube filament current of 20 mA and an accelerating voltage of 30 kV. Structural parameters were extracted from the reflectivity measurements using the REFS Mercury reflectivity autosimulation software from Bede, Inc.

E. Electron Probe Microanalysis. Electron probe microanalysis (EPMA) was carried out on a Cameca SX-50 at the University of Oregon. Elements were acquired using the following analyzing crystals: PET for W Mα, Si Kα; TAP for Al Kα, F Kα; and PC1 for O Kα. Data were collected at three different accelerating voltages (8, 10, and 12 keV) with experimental intensities determined from the average of 10 proximate positions on each sample. The standards were silicon metal for Si Kα, tungsten metal for W Mα, BaF_2 for F Kα, Al_2O_3 + 0.40 Cr single-crystal for Al Kα, and MgO for O Kα. Raw intensities were corrected using previously described procedures.[35] Quantitative elemental analysis was determined by comparing experimental k-ratios to simulated values using StrataGEM thin film composition analysis software that employs the PAP formalism.[36] The simulation employed a continuum correction for fluorescence and a correction to account for the carbon layer with a ∼20 nm thickness on the standards.

F. Secondary Ion Mass Spectrometry and Transmission Electron Microscopy. Secondary ion mass spectrometry (SIMS) profiles were conducted to investigate the chemical composition of the W/Al₂O₃ nanolaminates. These SIMS studies were performed at the Université de Bourgogne using a RIBER MIQ 256 instrument. These SIMS measurements used Ar^+ ions at 4 keV at 10° from the surface normal. In addition, a flooding technique employing $10^{−6}$ Torr of oxygen was used to enhance the secondary ion yields and to avoid the artificial increase of the tungsten signal at the Al_2O_3 interface. The sample was also rotated during the sputtering to improve the depth resolution according to the Zalar procedure.

(31) Groner, M. D.; Fabreguette, F. H.; Elam, J. W.; George, S. M. *Chem. Mater.* **2004**, *16*, 639.
(32) Juppo, M.; Rahtu, A.; Ritala, M.; Leskela, M. *Langmuir* **2000**, *16*, 4034.
(33) Ritala, M.; Leskela, M.; Dekker, J. P.; Mutsaers, C.; Soininen, P. J.; Skarp, J. *Chem. Vap. Deposition* **1999**, *5*, 7.
(34) Sauerbrey, G. *Z. Z. Phys.* **1959**, 206.

(35) Donovan, J. J.; Tingle, T. N. *Micro. Soc. Am.* **1996**, *2*, 1.
(36) Pouchou, J.; Pichoir, F. *Electron Probe Quantitation*; Heinrich, K. F. J., Newbury, D. E., Eds.; Plenum Press: New York, 1991; p 31.
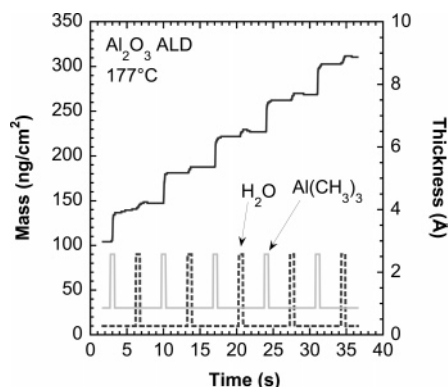
Figure 1. Quartz crystal microbalance measurements showing mass versus time and the Al(CH$_3$)$_3$ and H$_2$O timing sequence during Al$_2$O$_3$ ALD at 177 °C. The reactant exposure sequence was 1−5−1−5. The mass measurements were converted to Al$_2$O$_3$ thicknesses using an Al$_2$O$_3$ ALD density of 3.5 g/cm^3.

The transmission electron microscope (TEM) images were obtained by Dr. Jun Lu at the Ångstrom Laboratory at Uppsala University. These TEM images were acquired with a field-emission-gun TECNAI F30 ST operated at 300 kV. This instrument was equipped with a Gatan Imaging Filter and an EDAX energy-dispersive X-ray spectroscopy system.

G. Annealing of Nanolaminates. The thermal stability of the nanolaminates was studied by annealing in a Lindberg Hevi-Duty annealing oven at the University of Colorado. The thermal annealing was performed in a prepurified nitrogen environment from Air Gas Inc. The oven was first preheated to a desired temperature, and then the samples were placed into the heated zone of the oven. Samples were held at temperature for 1 h. Subsequently, the samples were allowed to cool under nitrogen for 15 min prior to exposure to ambient conditions. After annealing, the samples were tested using XRR techniques to evaluate the superlattice structure.

III. Results

Figure 1 displays in situ quartz crystal microbalance (QCM) results for cumulative mass change during Al$_2$O$_3$ ALD at 177 °C. The graph displays both the mass and thickness results versus time. The thicknesses were obtained from the mass results based on an Al$_2$O$_3$ ALD film density of 3.5 g/cm^3.[19] The growth rate achieved during steady-state Al$_2$O$_3$ ALD was 42 ng/cm^2/AB cycle. This mass gain per cycle corresponds to 1.2 Å/AB cycle. This Al$_2$O$_3$ ALD growth rate is in excellent agreement with previous ellipsometric and QCM measurements.[19,30]

The reactant pulse sequence is also displayed in Figure 1. The reactant exposure sequence was 1-s exposure of TMA, 5-s purge, 1-s exposure of H$_2$O, and 5-s purge. This reactant exposure sequence is designated 1−5−1−5 and the AB cycle time is 12 s. The TMA exposure was 1 × 10^5 Langmuir (1 Langmuir = 1 × 10^{-6} Torr s) during each 1-s exposure. The H$_2$O exposure was 5 × 10^4 Langmuir during each 1-s exposure. The QCM crystal experienced large mass increases during the TMA exposures. Much smaller mass increases are observed during the H$_2$O exposures.

Figure 2 shows the QCM results for cumulative mass change during W ALD at 177 °C. The graph displays both the mass and thickness results versus time. The thicknesses were obtained from the mass results based on a W ALD film density of 16.5 g/cm^3. The growth rate achieved during
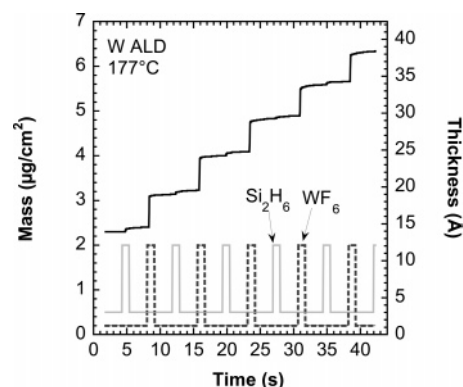

Figure 2. Quartz crystal microbalance measurements showing mass versus time and the Si$_2$H$_6$ and WF$_6$ timing sequence during W ALD at 177 °C. The reactant exposure sequence was 10−5−1−5. The mass measurements were converted to W thicknesses using an W ALD density of 16.5 g/cm^3.
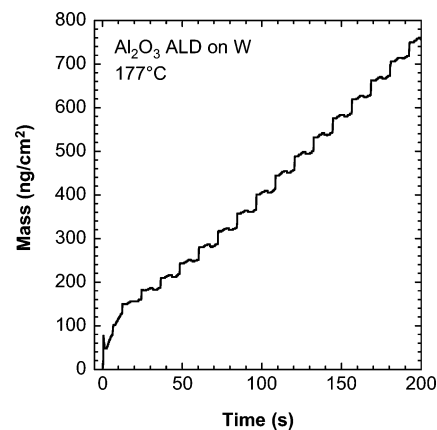

Figure 3. Mass versus time during the nucleation of Al$_2$O$_3$ ALD on W at 177 °C monitored by the quartz crystal microbalance. The time $t = 0$ corresponds to the beginning of Al$_2$O$_3$ ALD using a 1−5−1−5 reactant exposure. The previous W ALD layer was grown using a 10−5−1−5 sequence at 177 °C.

steady-state W ALD was 740 ng/cm^2/AB cycle. This mass gain per cycle corresponds to 4.5 Å/AB cycle. This W ALD growth rate agrees well with previous measurements that have been conducted under similar reaction conditions.[22,24−26,29]

The WF$_6$ and Si$_2$H$_6$ pulse sequence is also displayed in Figure 2. Large mass increases are observed during the WF$_6$ exposures. Much smaller mass increases are recorded during the Si$_2$H$_6$ exposures. Similar results were observed in previous QCM investigations.[29] The reactant exposure sequence used in this experiment was a 10-s Si$_2$H$_6$ exposure, 5-s purge, 1-s WF$_6$ exposure, and 5-s purge. This reactant exposure sequence is designated 10−5−1−5, and the AB cycle time is 21 s. The Si$_2$H$_6$ exposure was 2 × 10^6 Langmuir during each 10-s exposure. The WF$_6$ exposure was 2 × 10^5 Langmuir during each 1-s exposure.

To understand the growth of W/Al$_2$O$_3$ nanolaminates, the QCM can be utilized to investigate the nucleation of Al$_2$O$_3$ ALD on W surfaces and W ALD on Al$_2$O$_3$ surfaces. Figure 3 shows the mass changes during the nucleation of Al$_2$O$_3$ ALD on W at 177 °C. The TMA exposures were 1 × 10^5 Langmuir and the H$_2$O exposures were 5 × 10^4 Langmuir. The time $t = 0$ corresponds to the first TMA exposure onto the W surface following W ALD. The W ALD reactant exposure sequence ended with WF$_6$. A large mass increase is observed during the first TMA exposure. This large mass
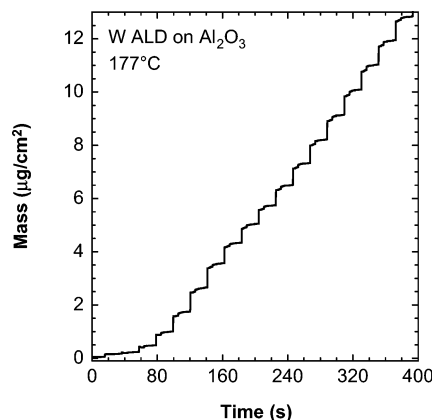
Figure 4. Mass versus time during the nucleation of W ALD on Al_2O_3 at 177 °C monitored by the quartz crystal microbalance. The time $t = 0$ corresponds to the beginning of W ALD using a $10-5-1-5$ reactant exposure. The previous Al_2O_3 ALD layer was grown using a $1-5-1-5$ sequence at 177 °C.
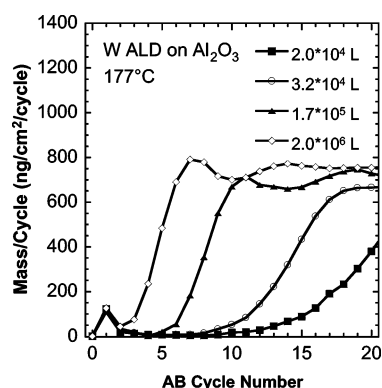

Figure 5. Quartz crystal microbalance measurements showing the mass change per AB cycle during W ALD on Al_2O_3 at 177 °C. The reactant exposure sequence was $X-5-1-5$. The Si_2H_6 exposures were measured in Langmuir (1 Langmuir = 10^{-6} Torr s).

gain indicates that Al_2O_3 ALD nucleates very quickly on the W surface.

Figure 4 shows the mass changes during the nucleation of W ALD on Al_2O_3 at 177 °C. The Si_2H_6 exposures were 2×10^6 Langmuir and the WF_6 exposures were 2×10^5 Langmuir. The time $t = 0$ corresponds to the first Si_2H_6 exposure onto the Al_2O_3 surface following Al_2O_3 ALD. The Al_2O_3 ALD reactant exposure sequence ended with H_2O. In contrast to the results for Al_2O_3 ALD on W, very little mass increase is observed during the first several AB cycles. The W ALD does not display facile nucleation on the Al_2O_3 surface. The W ALD steady-state growth rate of 740 ng/cm²/cycle is obtained only after six or seven AB cycles.

Figure 5 displays QCM results for the mass gain per cycle during W ALD on Al_2O_3. The mass gain per cycle provides a means to separate the nucleation region from the growth regime. Nucleation of W ALD on Al_2O_3 is studied for four different Si_2H_6 exposures. The Si_2H_6 exposures were varied by changing the Si_2H_6 exposure time at constant Si_2H_6 pressure. A Si_2H_6 exposure of 2×10^6 Langmuir corresponds to a 10-s exposure time at a Si_2H_6 pressure of 200 mTorr.

Figure 5 reveals that the nucleation of W ALD on Al_2O_3 is very sensitive to the Si_2H_6 exposures. In contrast, the nucleation of W ALD on Al_2O_3 was only weakly dependent on WF_6 exposures over a wide range of exposures. Higher
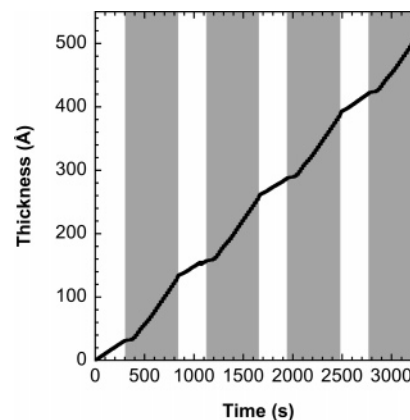

Figure 6. Thickness versus time during the growth of a four-bilayer W/Al_2O_3 nanolaminate at 177 °C monitored by the quartz crystal microbalance. The Al_2O_3 nanolayer was grown using 25 AB cycles with a $1-5-1-5$ reactant exposure sequence. The Al_2O_3 mass was converted to thickness using a density of 3.5 g/cm³. The W ALD nanolayer was grown using 25 AB cycles with a $10-5-1-5$ reactant exposure sequence. The W ALD mass was converted to thickness using a density of 16.5 g/cm³.

Si_2H_6 exposures reduced the number of AB cycles required to nucleate W ALD on Al_2O_3. The W ALD steady-state growth rate is obtained after six or seven AB cycles using a Si_2H_6 exposure of 2×10^6 Langmuir. Although the nucleation of W ALD is very sensitive to these Si_2H_6 exposures, the W ALD growth rate after W ALD nucleation is only slightly dependent on the Si_2H_6 exposure for this same set of Si_2H_6 exposures.[24] To ensure rapid nucleation of W ALD on Al_2O_3, the W/Al_2O_3 nanolaminates were grown using large Si_2H_6 exposures of 2×10^6 Langmuir.

An interesting oscillation in the mass deposited per cycle is revealed in Figure 5 versus AB cycle number. Recent simulations of ALD nucleation have observed that the growth per cycle can go through a maximum and then decrease to a steady-state value.[37] This maximum occurs during "substrate-inhibited growth of type 2" because of the difference in ALD growth rates on the initial substrate and on the ALD material.[37] In contrast, the maximum for W ALD growth per cycle is related to W island growth and the increase in W surface area that occurs with island growth prior to the coalescence of the W islands.[38] Maxima in the growth per cycle have also been monitored for Al_2O_3 ALD and ZrO_2 ALD on hydrogen-terminated Si(100).[39]

W/Al_2O_3 nanolaminates were then deposited at 177 °C using W ALD and Al_2O_3 ALD. The growth of the W/Al_2O_3 nanolaminate is shown in Figure 6. W ALD was performed using Si_2H_6 exposures of 2×10^6 Langmuir and WF_6 exposures of 2×10^5 Langmuir. Al_2O_3 ALD was performed using TMA exposures of 1×10^5 Langmuir and H_2O exposures of 5×10^4 Langmuir. To compare both W ALD and Al_2O_3 ALD, the observed mass changes were converted to thickness assuming a W ALD film density of 16.5 g/cm³ and an Al_2O_3 ALD film density of 3.5 g/cm³. Figure 6 shows

(37) Puurunen, R. L.; Vandervorst, W. *J. Appl. Phys.* **2004**, *96*, 7686.
(38) Wind, R. K.; Fabreguette, F. H.; George, S. M. Manuscript in preparation.
(39) Puurunen, R. L.; Vandervorst, W.; Besling, W. F. A.; Richard, O.; Bender, H.; Conard, T.; Zhao, C.; Delabie, A.; Caymax, M.; De Gendt, S.; Heyns, M.; Viitanen, M. M.; de Ridder, M.; Brongersma, H. H.; Tamminga, Y.; Dao, T.; de Win, T.; Verheijen, M.; Kaiser, M.; Tuominen, M. *J. Appl. Phys.* **2004**, *96*, 4878.

Table 1. XRR Measurements of the Al$_2$O$_3$ Layer Thickness, W Layer Thickness, and Total Film Thickness for the W/Al$_2$O$_3$ Nanolaminates Grown with Different Numbers of Bilayers and a Total Target Film Thickness of ~1000 Å[a]

no. of bilayers	Al$_2$O$_3$ layer (Å)	W layer (Å)	total film (Å)
2	311 (250)	262 (250)	1146
4	161 (125)	136 (125)	1189
8	83 (61)	74 (61)	1260
16	51 (31)	32 (31)	1335
32	25 (16)	19 (16)	1418
64	17 (8)	14 (8)	1964

[a] The numbers in parentheses are the predicted thicknesses based on the QCM results and assuming constant Al$_2$O$_3$ ALD and W ALD film densities.

Table 2. EPMA Measurements of the Atomic Percent of F, O, Al, and W in W/Al$_2$O$_3$ Nanolaminates Grown at 177 °C[a]

no. of bilayers	F	O	Al	W
2	1	33	25	40
4	2	36	24	38
8	3	36	23	36
16	7	35	22	36
32	12	27	17	44
64	19	16	12	54

[a] The W/Al$_2$O$_3$ nanolaminates were grown with different numbers of bilayers and a total target film thickness of ~1000 Å. The actual thicknesses are given in Table 1.
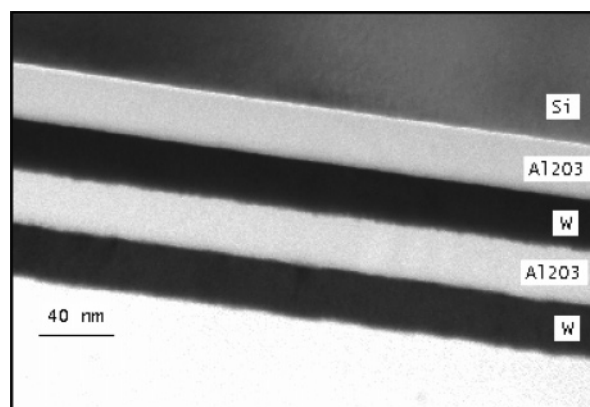
the progressive growth of the W/Al$_2$O$_3$ nanolaminate. The nucleation of Al$_2$O$_3$ ALD on W and W ALD on Al$_2$O$_3$ is repeatable for each W/Al$_2$O$_3$ bilayer in the W/Al$_2$O$_3$ nanolaminate.

On the basis of the results from the QCM investigations, W/Al$_2$O$_3$ nanolaminates were fabricated at 177 °C to obtain films with various numbers of bilayers and a total target thickness of ~1000 Å. XRR measurements were employed to characterize the individual layer thicknesses in the bilayers and the total film thickness. Each nanolaminate was grown using different numbers of AB cycles for W ALD and Al$_2$O$_3$ ALD to obtain the same total target thickness of ~1000 Å. For example, the 16-bilayer nanolaminate was deposited using 26 AB cycles of W ALD and 11 AB cycles of Al$_2$O$_3$ ALD for each bilayer. The 64-bilayer nanolaminate was deposited using five AB cycles of W ALD and six AB cycles of Al$_2$O$_3$ ALD for each bilayer.

The XRR measurements yielded the Al$_2$O$_3$ ALD layer thicknesses, W ALD layer thicknesses, and the total film thicknesses given in Table 1. The numbers in parentheses are the predicted thicknesses expected after the various numbers of AB cycles. The predicted thicknesses are based on the QCM investigations assuming a W ALD film density of 16.5 g/cm^3 and an Al$_2$O$_3$ ALD film density of 3.5 g/cm^3. Although the total film thickness was targeted to be ~1000 Å, the nanolaminates with higher interfacial density and larger number of bilayers were considerably thicker than ~1000 Å. A comparison between the predicted and measured layer thicknesses reveals that the larger total film thicknesses result primarily from larger than expected Al$_2$O$_3$ ALD layer thicknesses.

To understand the large discrepancy between the predicted and measured layer thicknesses, EPMA was conducted on these nanolaminates for atomic analysis. The results for the atomic percentages are shown in Table 2. The atomic percent of Si was <1% for all samples measured. The percentage of fluorine increases as the bilayer thickness decreases. Fluorine accounts for ~19% of the 64-bilayer W/Al$_2$O$_3$ nanolaminate. The correlation between the atomic percent of fluorine and the larger than predicted Al$_2$O$_3$ layer thicknesses suggests the existence of aluminum oxyfluoride layers with lower densities than expected for Al$_2$O$_3$ ALD layers.

A TEM image of a two-bilayer W/Al$_2$O$_3$ nanolaminate grown at 177 °C is shown in Figure 7. This two-bilayer nanolaminate was deposited using 225 AB cycles of Al$_2$O$_3$ ALD and 60 AB cycles of W ALD for each bilayer. A TEM

Figure 7. Transmission electron microscopy image of a two-bilayer W/Al$_2$O$_3$ nanolaminate grown at 177 °C. The Al$_2$O$_3$ nanolayer was grown using 225 AB cycles with a reactant exposure sequence of 1−5−1−5. The W nanolayer was grown using 60 AB cycles with a reactant exposure sequence of 10−5−1−5.
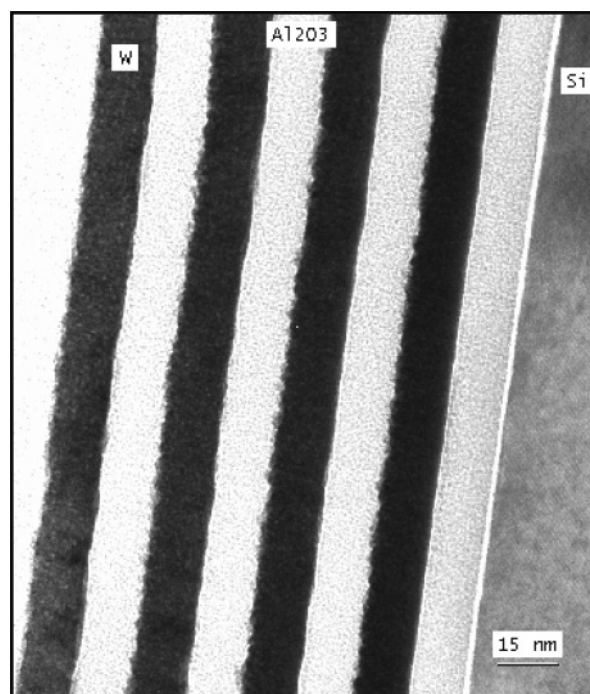

Figure 8. Transmission electron microscopy image of a four-bilayer W/Al$_2$O$_3$ nanolaminate grown at 177 °C. The Al$_2$O$_3$ nanolayer was grown using 111 AB cycles with a reactant exposure sequence of 1−5−1−5. The W nanolayer was grown using 32 AB cycles with a reactant exposure sequence of 10−5−1−5.

image of a four-bilayer W/Al$_2$O$_3$ nanolaminate grown at 177 °C is shown in Figure 8. This four-bilayer nanolaminate was deposited using 111 AB cycles of Al$_2$O$_3$ ALD and 32 AB
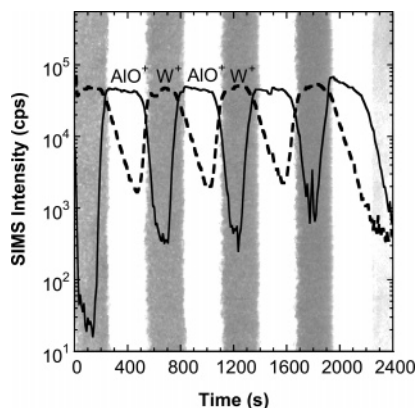
Figure 9. Secondary ion mass spectrometry (SIMS) measurements for a four-bilayer W/Al₂O₃ nanolaminate grown at 177 °C. The solid line shows the AlO⁺ signal and the dashed line designates the W⁺ signal. The TEM image in the background indicates the position of the W and Al₂O₃ nanolayers as a guide for the eye.

cycles of W ALD for each bilayer. The individual nanolayers in the W/Al₂O₃ nanolaminate are very clearly defined in each TEM image.

The TEM image in Figure 8 also shows a higher roughness at the interfaces where Al₂O₃ ALD is nucleating on W compared with the interfaces where W ALD is nucleating on Al₂O₃. This roughness may result from the polycrystallinity of the W ALD nanolayer and/or the W ALD nucleation on Al₂O₃. The TEM images in both Figures 7 and 8 also reveal a thin interfacial layer on the Si(100) substrate before the first Al₂O₃ nanolayer. This interfacial layer is probably SiO₂. This interfacial layer forms even though the starting Si(100) wafer was hydrogen-terminated after the HF solution treatment.[13,40]

SIMS measurements confirmed the chemical composition of the W/Al₂O₃ nanolaminates. SIMS results for a four-bilayer W/Al₂O₃ nanolaminate are shown in Figure 9. W⁺ and AlO⁺ were monitored using $m/z = 184$ and 43, respectively. The TEM image of the four-bilayer nanolaminate is also shown in the background for comparison. The W⁺ and AlO⁺ signals alternate as the incident Ar⁺ ions sputter through the W/Al₂O₃ nanolaminate.

In contrast to the TEM images, the SIMS measurements do not observe extremely sharp interfaces. There is some intermixing that is attributed to the finite resolution during Ar⁺ ion sputtering. However, the rise and fall of the SIMS intensities are not symmetrical for the interfaces where W ALD is nucleated on Al₂O₃ and Al₂O₃ ALD is nucleated on W. The AlO⁺ signal was used to obtain a qualitative understanding of these two interfaces. The interface resolution is defined as the sputtering time required for the AlO⁺ signal to change between 16% and 84% of its total value. These sputtering times defining the interface resolution for the four-bilayer W/Al₂O₃ nanolaminate are shown in Figure 10 for W ALD on Al₂O₃ and Al₂O₃ ALD on W.

The sputtering times are much shorter and the interface resolution is sharper for W ALD on Al₂O₃. This result is consistent with the TEM images that observed a sharper interface for W ALD nucleation on Al₂O₃. The shortest
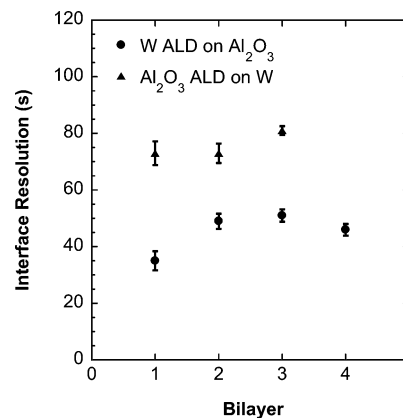
(40) Groner, M. D.; Elam, J. W.; Fabreguette, F. H.; George, S. M. *Thin Solid Films* **2002**, *413*, 186.

Figure 10. Interface resolution given in units of seconds as determined by the SIMS measurements in Figure 9. The solid circles represent the interface from W ALD on Al₂O₃. The solid triangles represent the interface from Al₂O₃ ALD on W. Bilayer 4 is the W/Al₂O₃ bilayer closest to the silicon substrate.
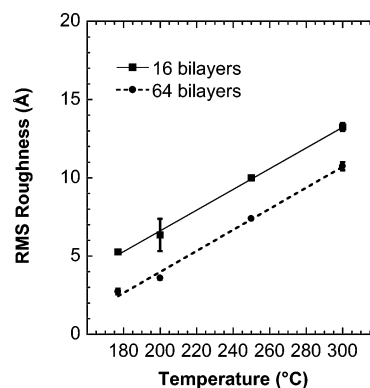

Figure 11. Surface root-mean-squared (rms) roughness as measured by noncontact atomic force microscopy. The solid squares show the AFM measurements of 16-bilayer nanolaminates. The solid circles show the AFM measurements of 64-bilayer nanolaminates.

sputtering time is observed for the first bilayer sputtered by the Ar⁺ ions. This top bilayer was the last bilayer deposited during the growth of the four-bilayer W/Al₂O₃ nanolaminate. The sputtering times increase for the first three bilayers, as expected given the finite resolution during Ar⁺ ion sputtering.

Surface roughness measurements were performed using AFM. These roughness measurements were performed on W/Al₂O₃ nanolaminates grown at different temperatures and with different interfacial densities. W/Al₂O₃ nanolaminates were grown with 1, 2, 4, 8, 16, 32, and 64 bilayers with a total target thickness of ∼1000 Å to evaluate the effect of interfacial density. The rms roughness of the 16- and 64-bilayer nanolaminates deposited at different growth temperature is shown in Figure 11.

The 64-bilayer nanolaminate with higher interfacial density has a much lower rms roughness at each growth temperature. The rms roughness is lower for the 64-bilayer nanolaminate even though this 64-bilayer nanolaminate was considerably thicker than the 16-bilayer nanolaminate. The rms roughness increases dramatically versus growth temperature. These results suggest that the W ALD nanolayers in the W/Al₂O₃ nanolaminates are more crystalline at higher growth temperatures and have larger crystallites in thicker W ALD nanolayers.

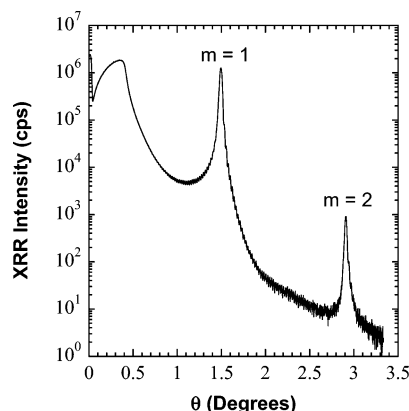3482   *Chem. Mater., Vol. 17, No. 13, 2005*

Sechrist et al.

Figure 12. X-ray reflectivity measurements from a 64-bilayer W/Al_2O_3 nanolaminate grown at 177 °C. Each bilayer had a thickness of ~30 Å.

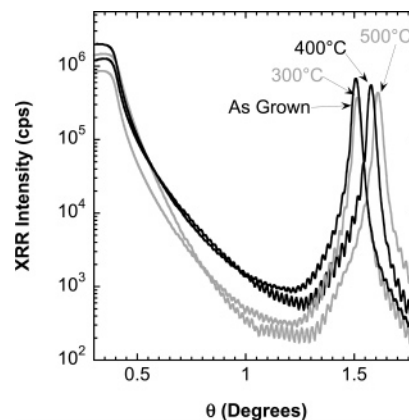**Figure 13.** X-ray reflectivity measurements from 64-bilayer W/Al_2O_3 nanolaminates after annealing. These W/Al_2O_3 nanolaminates were all grown using the same growth conditions as the 64-bilayer nanolaminate in Figure 12.

The XRR measurement of the 64-bilayer nanolaminate is shown in Figure 12. Two Bragg peaks and Kiessig fringes are apparent from this 64-bilayer nanolaminate. The first-order Bragg peak ($m = 1$) appears at 1.49° and the second-order Bragg peak ($m = 2$) appears at 2.92°. Using the REFS software, these Bragg angles indicate a bilayer thickness of 30 Å. The first-order Bragg peak has a very high reflectivity. However, the exact magnitude of this reflectance cannot be accurately quantified because the X-ray beam overfilled the W/Al_2O_3 nanolaminate sample. The large reflectivity indicates that the 64-bilayer W/Al_2O_3 nanolaminates may have potential application for X-ray mirrors.

The first Bragg peak can be used to monitor the thermal stability of the 64-bilayer W/Al_2O_3 nanolaminate. After growth of all the W/Al_2O_3 nanolaminates at 177 °C, the 64-bilayer W/Al_2O_3 nanolaminates were annealed to progressively higher temperatures. XRR measurements were performed after annealing at each of these higher temperatures. One nanolaminate was annealed at 200, 300, and then 600 °C. A second nanolaminate was annealed at 400, 500, and then 700 °C. A third nanolaminate was annealed only at 800 °C. Figure 13 shows the first-order Bragg peak versus annealing temperature. The first-order Bragg peak maintains its intensity for annealing temperatures as high as 500 °C. Subsequently, the nanolaminate films displayed cracks after annealing at ≥600 °C and the Bragg peak decayed in intensity. The peak is completely extinguished after annealing at 800 °C.

IV. Discussion

A. Nucleation during Al_2O_3 ALD on W and W ALD on Al_2O_3. The QCM measurements in Figure 3 reveal that the nucleation of Al_2O_3 ALD on W is very facile. A large mass gain is observed on the first TMA exposure to the W surface terminated with WF_4* surface species after W ALD. These results compare very favorably with recent Auger electron spectroscopy studies of Al_2O_3 ALD on W surfaces at 177 °C.[26] The Auger studies observed a large Al_2O_3 growth of 3.8 Å after the first AB cycle.[26] These studies were conducted in high vacuum and utilized an initial H_2O exposure on the W surface terminated with WF_4* species. The first TMA exposure led to a large Al_2O_3 deposition. Subsequent AB cycles led to an Al_2O_3 ALD growth rate of 1.0 Å/cycle.

The QCM results in this current study and the Auger results from the previous study are consistent with the rapid nucleation of Al_2O_3 ALD on W. Al_2O_3 ALD has the ability to nucleate quickly on a variety of surfaces, including oxides,[40,41] nitrides,[42] metals,[40] and polymers.[43,44] This ease of nucleation is probably related to facile nucleophilic attack by electron donors on TMA. In addition, the Al_2O_3 ALD chemistry using TMA and H_2O is very exothermic. The ability of TMA to adsorb on surfaces and absorb into the bulk of substrates leads to reactions between TMA and H_2O that form Al_2O_3 clusters that help to nucleate Al_2O_3 ALD.

In contrast to the nucleation of Al_2O_3 ALD on W, the nucleation of W ALD on Al_2O_3 is much more difficult. Figure 4 shows that very little mass gain is monitored during the first two or three AB cycles for W ALD on Al_2O_3 at 177 °C. The first several Si_2H_6 and WF_6 exposures do not effectively add mass to the Al_2O_3 surface. Mass gains are observed only after repeated Si_2H_6 and WF_6 exposures. The steady-state W ALD growth rate of 740 ng/cm^2/cycle is obtained only after six or seven AB cycles.

The nucleation of W ALD on Al_2O_3 is also very sensitive to the Si_2H_6 exposures, as illustrated by Figure 5. This dependence on Si_2H_6 exposure is consistent with an inefficient reaction between Si_2H_6 and −OH (hydroxyl) groups on the starting Al_2O_3 surface. A similar inefficient reaction between Si_2H_6 and hydroxyl groups on SiO_2 was observed by earlier Fourier transform infrared (FTIR) studies of W ALD on hydroxylated SiO_2 surfaces.[22] Lower Si_2H_6 exposures probably react with fewer −OH groups to deposit −$OSiH_2SiH_3$* surface species. WF_6 can then react with these Si surface species to deposit WF_4* surface species. The nucleation of W ALD is probably very dependent on the number of −$OSiH_2SiH_3$* surface species that are deposited by the Si_2H_6 exposure. The Si_2H_6 exposure can dramatically

(41) Damlencourt, J. F.; Renault, O.; Chabli, A.; Martin, F.; Semeria, M. N.; Bedu, F. *J. Mater. Sci.—Mater. Electron.* **2003**, *14*, 379.
(42) Ferguson, J. D.; Weimer, A. W.; George, S. M. *Thin Solid Films* **2000**, *371*, 95.
(43) Elam, J. W.; Wilson, C. A.; Schuisky, M.; Sechrist, Z. A.; George, S. M. *J. Vac. Sci. Technol. B* **2003**, *21*, 1099.
(44) Ferguson, J. D.; Weimer, A. W.; George, S. M. *Chem. Mater.* **2004**, *16*, 5602.

change the number of AB cycles required to reach the steady-state W ALD growth rate of ~740 ng/cm²/cycle.

These results are in good agreement with recent Auger electron spectroscopy (AES) studies of W ALD on Al₂O₃ surfaces at 177 °C.[26] The AES studies observed small W ALD growth rates of 0.8−1.0 Å/cycle for the first two or three AB cycles. Subsequently, the W ALD growth rate increased dramatically to 2.6−3.5 Å/cycle. This range of W ALD growth rates was determined from both the increasing W AES signals and the decreasing O AES signals from the underlying Al₂O₃ substrate during W ALD. Similar AES results were also observed for the nucleation of W ALD on SiO₂ surfaces.[25] In these studies, the W ALD required between nine and 10 AB cycles to nucleate on the underlying SiO₂ surface.[25]

The XRR results for the Al₂O₃ and W nanolayer thicknesses and total film thicknesses reveal that the Al₂O₃ ALD films are much thicker than expected for the nanolaminates with higher interfacial density and larger numbers of bilayers. These larger than expected layer thicknesses result primarily from lower densities for the thinner Al₂O₃ ALD nanolayers. The XRR thickness measurements and the corresponding QCM mass gains indicate that the Al₂O₃ ALD density starts at ~1.7 g/cm³ for an Al₂O₃ nanolayer layer thickness of 17 Å and increases to ~2.8 g/cm³ for an Al₂O₃ layer thickness of 311 Å. In addition, Table 2 reveals that the fluorine atomic percentage also increases with higher interfacial density and larger number of bilayers.

The lower density thin Al₂O₃ nanolayers may result from the formation of aluminum oxyfluoride. The formation of this aluminum oxyfluoride may occur during the WF₆ exposure on the Al₂O₃ surface. WF₆ can react with Al₂O₃ to produce AlF₃ according to the reaction Al₂O₃ + WF₆ → 2AlF₃ + WO₃. This exothermic reaction has a predicted reaction enthalpy of $\Delta H = -111$ kcal/mol according to the the *HSC Chemistry 5* thermochemical database from Outokumpu Research in Finland. The resulting thin layer may have a lower density than that observed for Al₂O₃ ALD.

Aluminum oxyfluoride films have been observed when Al₂O₃ films were exposed to fluorine species.[45,46] These investigations postulated a thin AlO$_x$F$_y$ layer on the surface of the Al₂O₃ film. The thin aluminum oxyfluoride layer may only form at the top of the Al₂O₃ ALD nanolayer. For the thin Al₂O₃ nanolayers in the 64-bilayer nanolaminates, this thin oxyfluoride layer may be a significant fraction of the Al₂O₃ nanolayer. For the thicker Al₂O₃ nanolayers in the nanolaminates with fewer bilayers, this oxyfluoride fraction of the Al₂O₃ nanolayers may become negligible. The larger fluorine atomic percentages for the thinner Al₂O₃ nanolayers support this interpretation.

The existence of an aluminum oxyfluoride layer was further supported by high concentrations of fluorine observed in the Al₂O₃ layers by Rutherford backscattering (RBS) at the University of Illinois at Urbana. The RBS measurements revealed that each Al₂O₃ layer contains a total fluorine atom concentration of ~3 × 10¹⁵ cm⁻².[8] The oxyfluoride layer

with lower density complicates the growth of W/Al₂O₃ nanolaminates with precise nanolayer thicknesses. The change of the density with layer thickness must be properly accounted for to obtain accurate Al₂O₃ ALD nanolayer thicknesses.

B. Growth and Structure of W/Al₂O₃ Nanolaminates. The TEM images in Figures 7 and 8 reveal very well defined W/Al₂O₃ nanolaminates. Very sharp interfaces are observed when W ALD nucleates on Al₂O₃ surfaces. Rougher interfaces result when Al₂O₃ ALD nucleates on W surfaces. This difference between the W/Al₂O₃ and Al₂O₃/W interfaces is also visible in the SIMS results given in Figures 9 and 10. On the basis of the Ar⁺ ion sputtering times, the W ALD on Al₂O₃ (W/Al₂O₃) interface is sharper than the Al₂O₃ ALD on W (Al₂O₃/W) interface.

The differences between the W/Al₂O₃ and Al₂O₃/W interfacial roughnesses can be explained on the basis of the nucleation difficulties and the structure of both nanolayers. Nucleation affects the interfacial roughness because W ALD does not nucleate easily on Al₂O₃. The nucleation period of six or seven AB cycles may lead to a rougher W ALD film on Al₂O₃. In addition, the W ALD is polycrystalline. The ALD of crystalline films leads to much rougher surfaces than the ALD of more amorphous films. These differences were clearly illustrated in previous surface roughness measurements of crystalline ZnO ALD and more amorphous Al₂O₃ ALD films.[9] The subsequent Al₂O₃ ALD on the underlying rough W ALD film will produce a rough Al₂O₃/W interface.

In contrast, Al₂O₃ ALD nucleates easily on W. Al₂O₃ ALD is also amorphous and will not produce additional surface roughness versus Al₂O₃ ALD film thickness. Moreover, the Al₂O₃ ALD film will act to smooth the roughness of the W ALD film. When the thickness of the Al₂O₃ ALD film exceeds one-half of the characteristic lateral length of the surface roughness, L, on the W surface, the Al₂O₃ ALD film will begin to smooth the surface roughness. This smoothing effect will continue for Al₂O₃ ALD film thicknesses $>L/2$. As a result, W ALD on this smoother Al₂O₃ ALD film will result in a sharper W/Al₂O₃ interface.

The sharper W/Al₂O₃ interface and rougher Al₂O₃/W interface are observed for all of the bilayers in the four-bilayer nanolaminate shown in Figure 8. This repetition is expected on the basis of the understanding of W ALD nucleation, polycrystalline W ALD film structure, and smoothing by Al₂O₃ ALD. The AFM measurements also show that the surface roughness is larger at higher growth temperatures. This larger surface roughness may be attributed to greater crystallinity of the W ALD films at higher temperatures. In addition, the rms roughness is greater for the 16-bilayer nanolaminates compared with the 64-bilayer nanolaminates. The larger W ALD thicknesses in the 16-bilayer nanolaminates lead to the growth of larger W crystallites that produce a rougher surface.

C. X-ray Reflectivity and Thermal Stability of W/Al₂O₃ Nanolaminates. Figure 12 reveals that the W/Al₂O₃ nanolaminates display excellent X-ray reflectivity. High X-ray reflectivities at $\lambda = 1.54$ Å (Cu Kα) are estimated from Figure 12. Unfortunately, absolute reflectivities could not be determined because the X-ray beam was overfilling the

(45) Chen, P. J.; Wallace, R. M.; Henck, S. A. *J. Vac. Sci. Technol., A* **1998**, *16*, 700.
(46) Kim, D. S.; Yu, Y. Y.; Char, K. *J. Appl. Phys.* **2004**, *96*, 2278.

W/Al_2O_3 nanolaminate sample. This high X-ray reflectivity is not unexpected, given the previous reports of X-ray mirrors made from various metal/Al_2O_3 superlattices.[47]

The W/Al_2O_3 superlattice is an excellent candidate as a hard X-ray mirror. Al_2O_3 is the spacer layer and W is the absorber layer. These two materials are a good combination because they have fairly small imaginary Fresnel reflection coefficients and different real Fresnel reflection coefficients.[48,49] The K-absorption edge of W sets the high-energy X-ray cutoff at 69.5 keV or 0.18 Å. At lower X-ray energies, the increasing absorption coefficients of W eventually limit the usefulness of the W absorber layer.

The W/Al_2O_3 nanolaminate may be an important hard X-ray mirror for high-temperature applications.[47] Both W and Al_2O_3 are refractory materials and should be resistant to moderate temperature excursions. The W/Al_2O_3 nanolaminate may be a useful candidate for X-ray mirrors for intense synchrotron beams and X-ray lasers.[50] In X-ray lasers, the X-ray mirrors are in close proximity to the hot plasma that emits the X-rays. The W/Al_2O_3 nanolaminate should have a much higher thermal stability than some of the other possible X-ray mirror candidates, such as the Mo/Si superlattice.

In addition to X-ray mirror applications, the W/Al_2O_3 nanolaminate may also have potential as a thermal barrier coating. Recent investigations revealed that the high interfacial density in W/Al_2O_3 nanolaminates led to decreased thermal conductivity.[8] Minimal thermal conductivities of ~0.55 W/mK at room temperature were achieved from a W/Al_2O_3 nanolaminate with a bilayer thickness of ~30 Å.[8] This thermal conductivity is a factor of ~3 less than the thermal conductivity of 1.3−3.0 W/mK at room temperature observed for amorphous oxides or strongly disordered crystalline oxides such as yttria-stabilized ZrO_2.[51−53]

For the W/Al_2O_3 nanolaminates to have application as X-ray mirrors or thermal barrier coatings, they need to be stable at higher temperatures. The observation of the first-order Bragg peak from the 64-bilayer nanolaminates was used as a measure of the thermal stability of the W/Al_2O_3 nanolaminates. Figure 13 shows that the first-order Bragg peak maintains its high intensity and shifts to slightly larger angles versus annealing temperature. The larger angles are attributed to smaller bilayer thicknesses after thermal annealing. These smaller bilayer thicknesses probably result from a shrinkage of the W and Al_2O_3 nanolayers. The second-order Bragg peak showed similar trends during annealing experiments that were performed using a high-temperature sample stage at the University of Oregon.

Annealing at 600 and 700 °C leads to film cracking and a pronounced change of shape and decrease of the diffraction peak. Annealing at 800 °C completely extinguishes the

diffraction peak. The loss of the first-order Bragg peak probably indicates that the superlattice structure has collapsed after annealing to 800 °C. This loss of superlattice structure could occur as a result of chemical mixing of the W and Al_2O_3 nanolayers. This chemical mixing would not be surprising, since the individual nanolayers have thicknesses of only 14 Å for the W nanolayer and 17 Å for the Al_2O_3 nanolayer in the W/Al_2O_3 bilayer.

Alternatively, the loss of the superlattice may result from the crystallization of the W nanolayer. If the W crystallites grow versus annealing, then the surface roughness of the W layer may increase and destroy the superlattice structure. The full width at half-maximum of the XRD peaks did decrease after annealing at higher temperatures, as expected for greater crystallite size. The growth of crystallites has also been used to explain the XRR results after thermal annealing for Ni/C,[54] Pt/C,[55] and Mo/C[56] X-ray multilayers.

V. Conclusions

The growth of W/Al_2O_3 nanolaminates using atomic layer deposition (ALD) techniques was optimized by employing quartz crystal microbalance (QCM) studies in a viscous flow reactor. The QCM results revealed that the fabrication of the nanolaminates was very dependent on nucleation and growth during the ALD of each layer. Al_2O_3 ALD on W nucleated quickly during the first AB reaction cycle. W ALD nucleation on Al_2O_3 required multiple WF_6/Si_2H_6 reaction cycles and was very sensitive to the Si_2H_6 exposure. An oscillation in the mass deposited per cycle may be related to W island growth and the increase in W surface area that occurs with island growth prior to the coalescence of the W islands. The density of the Al_2O_3 ALD layer in the W/Al_2O_3 nanolaminates was also lower than expected for thin Al_2O_3 nanolayers. These nucleation difficulties and density changes complicate the growth of W/Al_2O_3 nanolaminates with precise thicknesses.

TEM images showed that the optimum growth conditions led to very well-defined W/Al_2O_3 nanolaminates at 177 °C. The composition of these W/Al_2O_3 nanolaminates was confirmed by secondary ion mass spectrometry measurements. The TEM images also revealed that sharper interfaces were observed when W ALD nucleates on Al_2O_3 and rougher interfaces were observed when Al_2O_3 ALD nucleates on W. These different interfacial roughnesses were explained by nucleation difficulties for W ALD on Al_2O_3, the polycrystalline W ALD layers, and the smoothing effect of the Al_2O_3 ALD layers.

XRR investigations revealed a very pronounced Bragg peak that yielded a high X-ray reflectivity from 64-bilayer W/Al_2O_3 nanolaminates grown at 177 °C. The X-ray reflectivity intensity of the 64-bilayer W/Al_2O_3 nanolaminates grown at 177 °C was constant versus annealing to 500 °C. The reflectivity then decreased for annealing at ≥600 °C.

(47) Morawe, C.; Zabel, H. *J. Appl. Phys.* **1996**, *80*, 3639.
(48) Ishino, M.; Yoda, O. *Appl. Opt.* **2004**, *43*, 1849.
(49) Yamamoto, M.; Namioka, T. *Appl. Opt.* **1992**, *31*, 1622.
(50) Ziegler, E.; Lepetre, Y.; Joksch, S.; Saile, V.; Mourikis, S.; Viccaro, P. J.; Rolland, G.; Laugier, F. *Rev. Sci. Instrum.* **1989**, *60*, 1999.
(51) Lee, S. M.; Cahill, D. G.; Allen, T. H. *Phys. Rev. B* **1995**, *52*, 253.
(52) Hasselman, D. P. H.; Johnson, L. F. *J. Compos. Mater.* **1987**, *21*, 508.
(53) Schlichting, K. W.; Padture, N. P.; Klemens, P. G. *J. Mater. Sci.* **2001**, *36*, 3003.

(54) Lodha, G. S.; Pandita, S.; Gupta, A.; Nandedkar, R. V.; Yamashita, K. *J. Electron. Spectrosc. Relat. Phenom.* **1996**, *80*, 453.
(55) Lodha, G. S.; Pandita, S.; Gupta, A.; Nandedkar, R. V.; Yamashita, K. *Appl. Phys. A* **1996**, *62*, 29.
(56) Suresh, N.; Modi, M. H.; Tripathi, P.; Lodha, G. S.; Chaudhari, S. M.; Gupta, A.; Nandedkar, R. V. *Thin Solid Films* **2000**, *368*, 80.

This thermal instability will place some limits on the application of W/Al$_2$O$_3$ nanolaminates as thermal barrier coatings and X-ray mirrors.

CM050470Y